First Study of the Pyrolysis of a Halogenated Ester: Methyl Chloroacetate

Nicolas Vin, Frédérique Battin-Leclerc, Olivier Herbinet

First Study of the Pyrolysis of a Halogenated Ester: Methyl Chloroacetate

Nicolas Vin[1,2], Frédérique Battin-Leclerc[1], Olivier Herbinet[1,*]

[1]Laboratoire Réactions et Génie des Procédés, CNRS, Université de Lorraine, BP 20451, 1 rue Grandville, 54000 Nancy, France.

[2]Terbis, 943 rue Pasteur, 60700 Pont Sainte Maxence, France

* Corresponding author: olivier.herbinet@univ-lorraine.fr

Published in Industrial & Engineering Chemistry Research (ACS), 2019, 58, 22, 9331-9338

Abstract

The pyrolysis of a halogenated ester, methyl chloroacetate (MC), under dilute atmosphere and quasi-atmospheric pressure was studied at temperatures from 473 to 1048 K using an alumina tubular reactor. MC was chosen as a surrogate to model the thermal decomposition of ethyl bromoacetate, a chemical warfare agent. A maximum MC conversion of 99.8% was observed at a residence time of 2 s, a temperature of 1048 K, and an inlet mole fraction of 0.01. The following products were quantified: CO, CO_2, HCl, methane, ethylene, ethane, propene, chloromethane, dichloromethane, vinyl chloride, chloroethane, and dichloroethane. For the first time, a detailed kinetic model of MC pyrolysis was developed and gave a good prediction of the global reactivity and the formation of most of the major products. Flow rate and sensitivity analyses were made to highlight the different pathways of decomposition during the MC pyrolysis. In a first attempt to extrapolate the results obtained with methyl chloroacetate to ethyl bromoacetate, simulations were run with a modified version of the model developed in this study taking into account the differences in bond dissociation energies induced by the change of the chlorine atom by a bromine one.

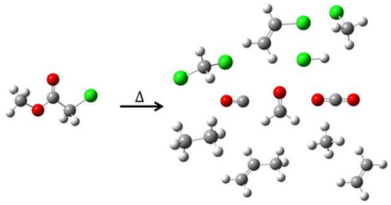

1. Introduction

Methyl chloroacetate (MC) is a halogenated ester mainly used as a solvent in organic synthesis or in the preparation of several compounds [1,2]. Typically, MC is used in the preparation of (carboxymethyl) trimethylammonium chloride esters [3] or in the synthesis of octakis-(carbethoxymethoxy)calix[8]arene [4]. Additionally, methyl chloroacetate acts as an extraction solvent during the separation of neutral compounds with concentration enhancement using coupling liquid–liquid semi-microextraction with micellar electrokinetic chromatography through on-capillary decomposition [5]. The destruction of the stock of toxic chemical warfare agents, absorbed in soils or stored as unexploded ammunitions, is still an environmental challenge in many countries [6,7]. The destruction of these dangerous compounds by pyrolysis can be a valuable alternative to their incineration [8], because the absence of oxygen limits the amount of exhausted gases to be treated at the outlet of such a process and disfavors the possibility of dioxin or furan formations [9]. In this work, methyl chloroacetate (see structure in Figure 1) has been chosen as a nonhazardous surrogate of more toxic ethyl bromoacetate (see structure in Figure 1) in order to better evaluate the possible thermal decomposition of this well-known chemical warfare used as a lachrymatory and tear gas agent during the First World War.

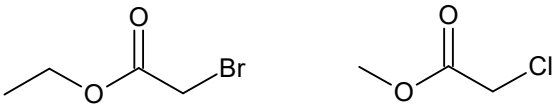

Figure 1. Structures of ethyl bromoacetate and of methyl chloroacetate.

Unless we are mistaken, no study was performed yet on the pyrolysis or oxidation of methyl chloroacetate. However, recent experimental works on the pyrolysis and oxidation of methyl acetate are available in the literature [10–13]. Farooq et al. [10] in 2009 studied the high temperature decomposition of methyl acetate behind reflected shock waves over the range 1260–1653 K, at pressures of 1.4–1.7 atm, providing new experimental data. In 2012, Peukert et al. [11] studied the thermal decomposition of methyl acetate in a shock tube between 1194 and 1371 K at 0.5 bar. The authors show that the two major unimolecular initiations are:

$$CH_3OC(O)CH_3 \rightarrow CH_3 + OC(O)CH_3$$

$$CH_3OC(O)CH_3 \rightarrow CH_3 + CH_3OCO$$

Additionally, the study highlights two molecular reactions leading to the formation of the same products: methanol and ketene. Furthermore, the H-atom abstractions are important in the system.

Yang et al. [12] investigated the chemistry of the combustion of methyl acetate first in a flow reactor between 500 and 1150 K at atmospheric pressure and then with use of a flat flame burner at low pressure with molecular-beam mass spectrometry. Ab initio calculations have been performed to determine the rate constants of the H-atom abstraction from methyl chloroacetate by O, H, OH, CH_3, and HO_2 radicals. A detailed kinetic model was developed. In the flow reactor, the two major ways of decomposition lead to the formation of $CH_3 + CH_3 + CO_2$ and $CH_3OH + CH_2CO$. Identified products are ethane, formaldehyde, methanol, CO, and CO_2. Flame experiments suggest a unique channel of decomposition yielding to the formation of aldehydes, ketones, and several carboxylic acids. Ren et al. [13] have studied the pyrolysis (between 1401 and 1605 K) and the oxidation (between 1423 and 1674 K) of methyl acetate in a shock tube at 1.5 bar. In this work, the main decomposition pathway of methyl acetate was:

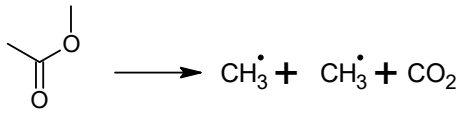

Minor decomposition pathways include the breaking of the C–O bond (giving CH_3OCO and CH_3 radicals) and a molecular decomposition yielding methanol and ketene, as written before in the study of Peukert et al. [11]. A modified version of the detailed kinetic model developed by Yang et al. [12] leads to good agreement with these shock tube data.

2. Materials and Methods

The present experimental procedure was already used to study the pyrolysis of chlorobenzene [14] and bromoéthane [15]. Since this procedure has been already detailed in these previous works, reminders of only the main features are given here. A scheme of the experimental setup is given in the Supplementary Material (Figure S1). Experimental studies in the tubular reactor (TR) have been performed using a horizontal 60 cm long alumina tube (volume of 294 cm^3). The ends of the reactor were connected to 2.54 cm (1 inch) diameter Swagelok unions and sealed with high temperature epoxy resin from Final Crotonics. The tubular reactor was inserted in an electrical furnace from Vecstar and equipped with an S-type thermocouple. For each set reaction temperature, a temperature profile (temperature versus position in the tubular reactor) was measured using an S-type thermocouple (see measured profiles in Figure S2 in the Supplementary Material). Experiments were performed at a constant pressure of 1.067 bar, at a residence time in the set-point temperature zone around 2 s, and at temperatures ranging from 473 to 1048 K with high dilution in helium. Simulations

were performed assuming that the TR can be modeled as a plug flow reactor in our operating conditions and using the measured temperature profiles as an input. The assumption of the plug flow reactor has already been checked in a previous study [15].

Helium was provided by Messer (purity of 99.999%), and MC was purchased from Sigma-Aldrich (purity of 99.0%). Gas flow rates were controlled by mass flow controllers and the liquid flow rate by a Coriolis flow controller. The uncertainty in the flow measurements was around 0.5% for each controller, so about 1% on the residence time.

Using a heated transfer line maintained at 433 K to avoid product condensation, the gases leaving the reactors were analyzed using the following:

- Gas chromatography (GC) for a first chromatograph, fitted with a PlotQ capillary column, a thermal conductivity detector (TCD), and a flame ionization detector (FID), was used for the quantification of light products and the reactant; a second chromatograph, fitted with a HP-1 capillary column and a FID, was used for the quantification of heavier products. The identification of reaction products was performed using a gas chromatograph equipped with a PlotQ capillary column and coupled to a mass spectrometer. Response factors were determined by injecting calibration mixtures or using the effective carbon number method. Relative uncertainties in mole fractions were estimated to be ±5% for species which were calibrated using standards and ±10% for other ones.
- Fourier transform infrared spectrometer (FTIR) from Thermo Scientific Antaris was equipped with a Mercure Cadmium Tellure photoelectric detector. FTIR was used to identify and quantify MC, HCl, formaldehyde, CO, and CO_2. FTIR calibrations were obtained by injecting standards. Relative uncertainties can be slightly higher than in GC since interferences may occur between bands of absorbing species.

3. Kinetic Model Development

Simulations were performed using the OpenSMOKE package [16], and for the first time, a detailed chemical kinetic reaction mechanism for methyl chloroacetate pyrolysis has been developed. This mew model was based on the widely used C_0–C_4 core mechanism Aramco Mech 2.0 [17], which included the kinetic model published by Ren et al. [13] for methyl acetate oxidation. To model the chlorinated reactant, the reactions of the H/Cl system involving HCl, Cl_2, and Cl radicals taken from

Pelucchi et al. [18] were added, as well as reactions specific to methyl chloroacetate pyrolysis, which are listed in Table 1. The final mechanism includes 519 species involved in 2857 reactions (given in the Supplementary Material under Chemkin format).

Table 1. Reactions Rate Constants Added to the Core Mechanism[a]

reaction	A	n	E_a	footnote	ref.
unimolecular initiations					
$CH_3OCOCH_2Cl = CH_3 + COOCH_2Cl$	4.6×10^{35}	−19.6	126000	b	[1]
$CH_3OCOCH_2Cl = Cl + CH_3OCOCH_2$	1.0×10^{15}	0.0	738000	c	[2]
$CH_3OCOCH_2Cl = CH_2Cl + CH_3OCO$	1.9×10^{77}	−17.8	126064	d	[3]
$CH_3OCOCH_2Cl = COCH_2Cl + CH_3O$	0.7×10^{16}	0.0	193645	e	[4]
$CH_3OCOCH_2Cl = CH_3 + CH_2Cl + CO_2$	2.0×10^{79}	−18.0	123552	e	[5]
metathesis with H					
$CH_3OCOCH_2Cl + H \Rightarrow CH_3OCOCH_2 + HCl$	5.2×10^{07}	2.03	8061	f	[6]
$CH_3OCOCH_2 + HCl \Rightarrow CH_3OCOCH_2Cl + H$	4.8×10^{05}	2.18	33748	f	[7]
$CH_3OCOCH_2Cl + H \Rightarrow CH_3OCOCHCl + H_2$	2.0×10^{06}	2.36	5838	f	[8]
$CH_3OCOCHCl + H_2 \Rightarrow CH_3OCOCH_2Cl + H$	6.2×10^{06}	1.93	19184	f	[9]
$CH_3OCOCH_2Cl + H \Rightarrow CH_2OCOCH_2Cl + H$	7.3×10^{02}	2.60	8563	f	[10]
$CH_2OCOCH_2Cl + H \Rightarrow CH_3OCOCH_2Cl + H$	7.0×10^{06}	1.60	13352	f	[11]
metathesis with CH_3					
$CH_3OCOCH_2Cl + CH_3 \Rightarrow CH_3OCOCH_2 + CH_3Cl$	4.5×10^{03}	2.88	12523	f	[12]
$CH_3OCOCH_2 + CH_3Cl \Rightarrow CH_3OCOCH_2Cl + CH_3$	2.0×10^{05}	2.42	19971	f	[13]
$CH_3OCOCH_2Cl + CH_3 \Rightarrow CH_3OCOCHCl + CH_4$	7.5×10^{01}	3.24	5937	f	[14]
$CH_3OCOCHCl + CH_4 \Rightarrow CH_3OCOCH_2Cl + CH_3$	1.8×10^{03}	3.12	19477	f	[15]
$CH_3OCOCH_2Cl + CH_3 \Rightarrow CH_2OCOCH_2Cl + CH_4$	8.0×10^{01}	3.42	10091	f	[16]
$CH_2OCOCH_2Cl + CH_4 \Rightarrow CH_3OCOCH_2Cl + CH_3$	6.1×10^{03}	2.73	15077	f	[17]
metathesis with Cl					
$CH_3OCOCH_2Cl + Cl = CH_3OCOCH_2 + Cl_2$	1.2×10^{09}	1.63	25400	g	[18]
$CH_3OCOCH_2Cl + Cl \Rightarrow CH_3OCOCHCl + HCl$	9.0×10^{03}	3.04	−3929	f	[19]
$CH_3OCOCHCl + HCl \Rightarrow CH_3OCOCH_2Cl + Cl$	6.5×10^{03}	2.51	8474	f	[20]
$CH_3OCOCH_2Cl + Cl \Rightarrow CH_2OCOCH_2Cl + HCl$	1.1×10^{02}	3.72	−3958	f	[21]
$CH_2OCOCH_2Cl + HCl \Rightarrow CH_3OCOCH_2Cl + Cl$	2.4×10^{02}	2.63	−113	f	[22]
metathesis with CH_2Cl					
$CH_3OCOCH_2Cl + CH_2Cl \Rightarrow CH_3OCOCH_2 + CH_2Cl_2$	0.4×10^{03}	2.88	12523	g	[23]
$CH_3OCOCH_2 + CH_2Cl_2 \Rightarrow CH_3OCOCH_2Cl + CH_2Cl$	0.5×10^{05}	2.42	19971	g	[24]
$CH_3OCOCH_2Cl + CH_2Cl \Rightarrow CH_3OCOCHCl + CH_3Cl$	1.9×10^{01}	3.24	5935	g	[25]
$CH_3OCOCHCl + CH_3Cl \Rightarrow CH_3OCOCH_2Cl + CH_2Cl$	0.3×10^{03}	3.12	19477	g	[26]
$CH_3OCOCH_2Cl + CH_2Cl \Rightarrow CH_2OCOCH_2Cl + CH_3Cl$	2.0×10^{03}	3.42	10091	g	[27]
$CH_2OCOCH_2Cl + CH_3Cl \Rightarrow CH_3OCOCH_2Cl + CH_2Cl$	1.5×10^{03}	2.73	15077	g	[28]
β-scission					
$CH_3OCOCHCl = COCHCl + CH_3O$	5.5×10^{13}	0.66	49300	h	[29]
$COOCH_2Cl \Rightarrow CH_2Cl + CO_2$	8.7×10^{17}	−1.81	13657	i	[30]
$CH_2OCOCH_2Cl \Rightarrow CH_2O + COCH_2Cl$	5.5×10^{07}	1.57	28908	f	[31]
$CH_2O + COCH_2Cl \Rightarrow CH_2OCOCH_2Cl$	6.4×10^{-02}	3.65	7304	f	[32]
α-scission					

reaction	A	n	E_a	footnote	ref.
$COCH_2Cl \Rightarrow CO + CH_2Cl$	2.3×10^{15}	–0.33	14186	f	[33]
$CO + CH_2Cl \Rightarrow COCH_2Cl$	1.5×10^{06}	1.71	7410	f	[34]
isomerizations					
$CH_3OCOCHCl \Rightarrow CH_2OCOCH_2Cl$	4.7×10^{06}	1.84	30594	f	[35]
$CH_2OCOCH_2Cl \Rightarrow CH_3OCOCHCl$	2.2×10^{07}	1.27	22037	f	[36]
terminations					
$CH_2Cl + H = CH_3Cl$	1.0×10^{14}	0.0	0.0	j	[37]
$CH_2Cl + Cl = CH_2Cl_2$	1.0×10^{13}	0.0	0.0	j	[38]
$CH_2CH_2Cl + H = C_2H_5Cl$	1.0×10^{14}	0.0	0.0	j	[39]
$CH_2CCl + H = CH_2CHCl$	1.0×10^{14}	0.0	0.0	j	[40]
other reactions					
$COCHCl + Cl \Rightarrow CO + CHCl_2$	1.5×10^{14}	0.0	0.0	k	[41]
$COCHCl + H \Rightarrow CO + CH_2Cl$	7.8×10^{08}	1.45	2780	l	[42]

[a] Note that kinetic parameters are given under the following form: $k = AT^n \exp(-E_a/RT)$ with A in $cm^{-3}\cdot mol^{-1})^{p-1}\cdot s^{-1}$ with p being the reaction order, T in kelvin, and E_a in calories per mole.

[b] Rate constants estimated by those of the reaction $CH_3OCOCH_3 = CH_3 + CH_3OCO$ [11].

[c] Rate constants estimated by those of the reaction $CH_3Cl = CH_3 + Cl$ [24].

[d] Rate constants estimated by those of the unimolecular initiation of ethyl acetate [13].

[e] Rate constants estimated by those of the unimolecular initiation of methyl undecanoate determined by KINGAS [30].

[f] Rate constants calculated using quantum methods.

[g] Rate constants estimated by those of the H-atom abstraction on methyl chloroacetate by methyl radicals.

[h] Rate constants estimated by those of the reaction $CH_2OCOCH_3 = CH_2CO + CH_3O$ [31].

[i] Rate constants estimated by those of the reaction $CH_3OCO = CH_3 + CO_2$ [32].

[j] Rate constants estimated by those of terminations generated by KINGAS [30].

[k] Rate constants estimated by those of the reaction $COCH_2 + Cl = CO + CH_2Cl$ [33].

[l] Rate constants estimated by those of the reaction $COCH_2 + H = CO + CH_3$ [34].

For some reactions of Table 1, rate parameters were estimated by analogy with similar reactions. Calculations using quantum methods were carried out when no data were available. Calculations of kinetic constants were carried out using the Gaussian 09 revision B.01 suite of programs [19] (at the CBS-QB3 level [20]) following a classical procedure. The conformational analysis was performed to check that optimized structures corresponded well to global minima (at the B3LYP/6-31G(d) level [21]). Internal rotations of moieties around simple bonds in optimized species have been treated like hindered rotors, and their contribution were considered in kinetic parameter calculations through the calculation of partition functions. Intrinsic reaction coordinate calculations were performed to check that transition states well-connected both reactants and products. Rate constants were obtained thanks to the transition state theory using Gibbs energies of species involved in the considered reaction. They were corrected to take into account the tunneling (using the asymmetric Eckart potential). The Fancy software from Carstensen [22] was used to perform the post-treatment

of the Gaussian calculations. Energies, frequencies, and coordinates of calculated species are given in the Supporting Information. Note that kinetic parameters calculated for reaction 30 in Table 1 are in good agreement with data previously calculated by Mereau et al. [23] (see Supplementary Material for the comparison).

The following types of reactions were added to account for the reactant consumption:

- Unimolecular initiation reactions by breaking C–C or C–O bonds whose rate parameters were taken equal to the unimolecular initiation reactions in methyl acetate [13] (reactions 1, 3, 4, and 5 in Table 1). The rate parameters for the unimolecular initiations by breaking the C–Cl bond in MC has been estimated as those of $CH_3Cl = CH_3 + Cl$ [24] (reaction 2 in Table 1).
- Cl-atom abstraction by H atoms (reaction 6 in Table 1), by methyl radicals (reaction 12 in Table 1), and by Cl atoms (reaction 18 in Table 1) and H-atom abstractions by H atoms (reactions 8 and 10 in Table 1), by methyl radicals (reactions 14 and 16 in Table 1), and by Cl-atoms (reactions 19 and 21 in Table 1) with all the related reverse reactions. The rate constants of the abstractions by chloromethyl radical were taken equal to those by methyl radical with a pre-exponential factor divided by a factor of 4 (reactions 23–28 in Table 1).
- β-scission decomposition of the fuel radical CH_2OCOCH_2Cl and reverse reaction (reactions 31 and 32 in Table 1).
- α-scission decomposition of the $COCH_2Cl$ radical and reverse reaction (reactions 33 and 34 in Table 1).
- Reactions of isomerization between CH_2OCOCH_2Cl and $CH_3OCOCHCl$ radicals (reactions 35 and 36 in Table 1).
- Reactions of termination yielding chloromethane, dichloromethane, chloroethane, and vinyl chloride (reactions 37–40 in Table 1).

The thermodynamic data of all the species of the mechanism can be found in the “thermo” .txt file (Supplementary Material). The thermodynamic data of the species involved in the reactions of Table 1 were taken from the database of Burcat [25] taken from the literature [18] determined by ab initio calculations, or calculated by the Thergas software [26] based on group additivity method (the reader can refer to the file for the origin of the thermodynamic properties).

4. Results and Discussion

This part presents the main results obtained during the pyrolysis of MC in the TR. The evolution of the fuel conversion is first presented. Furthermore, the nature of the reaction products and the evolution of their mole fractions are discussed.

4.1. Methyl Chloroacetate Conversion

Figure 2 presents experimental and simulated evolutions with temperature and residence time of the MC conversion obtained in the TR.

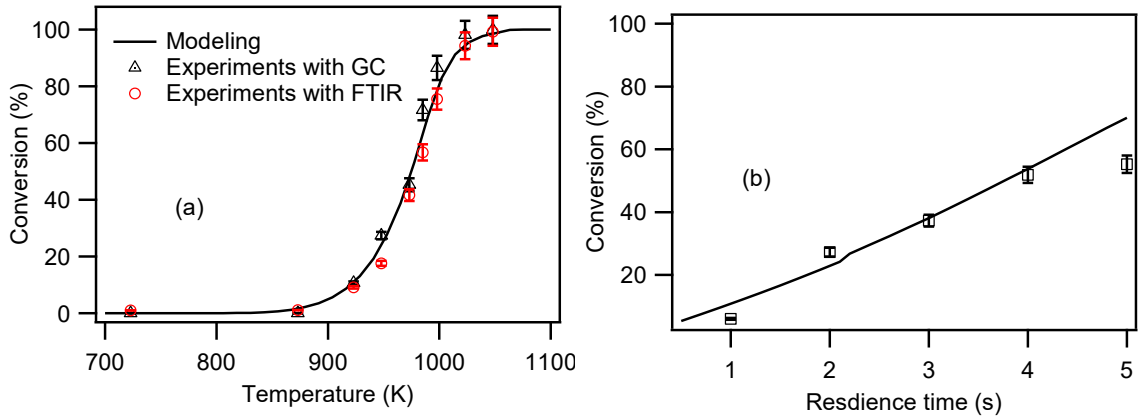

Figure 2. (a) Evolution with temperature of MC conversion (MC inlet mole fraction of 0.01, residence time of 2 s, and P = 1.07 bar); (b) evolution with residence time of MC conversion (948 K, MC inlet mole fraction of 0.01, and P = 1.07 bar). Symbols are experiments obtained by GC and FTIR, and lines, simulations.

The onset temperature for the MC molecule is 875 K. The maximum conversion in the TR (99.8%) was encountered at 1048 K, the highest studied temperature, as is shown in Figure 2a. Figure 2b shows a significant impact of the residence time on the conversion of MC in the TR since a rise of the residence time from 1 to 5 s led to an increase of the conversion from 6.0% to 55.3%.

The model reproduces very well the experimental results for the variations of the MC conversion with temperature and residence time under our operating conditions.

4.2. Product from the MC Pyrolysis

This part focuses on the experimental and computed results for the products obtained during the MC pyrolysis. First, a product selectivity diagram at 998 K is plotted in Figure 3 and shows that CO, chloromethane, methane, and HCl are the major products during the pyrolysis of MC at 998 K.

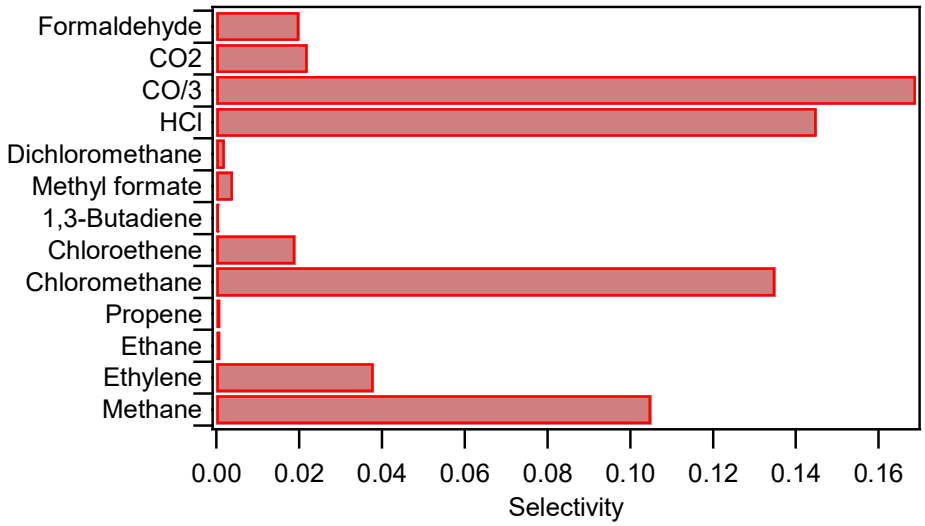

Figure 3. Selectivity of reaction products obtained during the MC pyrolysis in the TR (998 K, MC inlet mole fraction of 0.01, residence time of 2 s, and P = 1.07 bar). The selectivity of CO has been divided by 3.

HCl, CH_4, H_2O, CH_2O, CO_2, and CO were identified and quantified by FTIR spectroscopy. These species can be seen in Figure 4, which shows an infrared spectrum recorded at 973 K during the pyrolysis of MC in the TR. Interferences are visible in Figure 4 between the bands of absorption of CH_4, CH_2O, and HCl, involving higher uncertainties for the quantification of CH_2O and HCl (CH_4 was also quantified by GC).

Traces of dichloroethane, dichloroethene, ethyl acetate, methanol, acetaldehyde, 1,3-butadiene, allyl chloride, and water were also detected. Below 973 K, carbon-, oxygen-, and chlorine-atom balances are satisfactory. Beyond this temperature, we observe a slight deviation especially for the chlorine-atom balance (see Table S1 in the Supplementary Material).

The experimental data are then compared with the computed results, as shown in Figure 5. The kinetic model developed in this study predicts well the formation of CO, chloromethane, dichloromethane, and CO_2. The formation of formaldehyde is overestimated by the model as well as the formation of methane, HCl, and propene for temperatures higher than 1000 K. Contrariwise, the formation of ethylene and vinyl chloride is underestimated. The important numbers of estimated kinetic parameters used in the model could partly explain the observed deviations between computed and experimental data. Furthermore, uncertainties are higher for the experimental mole fraction of CH_2O and HCl due to interferences (see Figure 4).

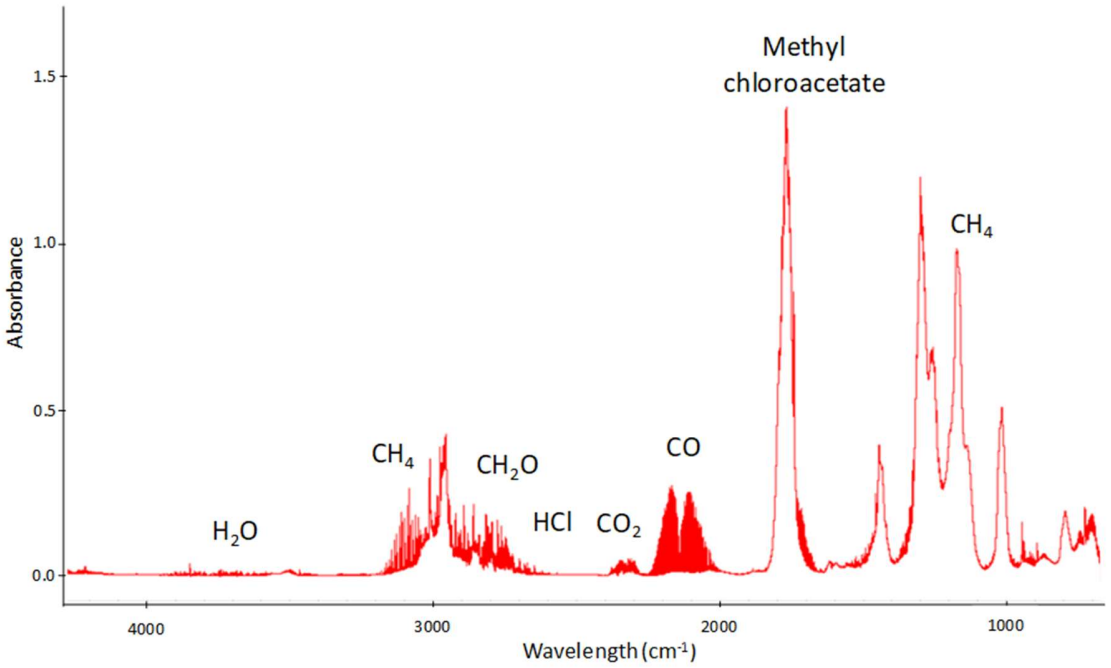

Figure 4. Infrared spectrum obtained by FTIR spectroscopy during the pyrolysis of MC in the TR (973 K, MC inlet mole fraction of 0.01, residence time of 2 s, and P = 1.07 bar).

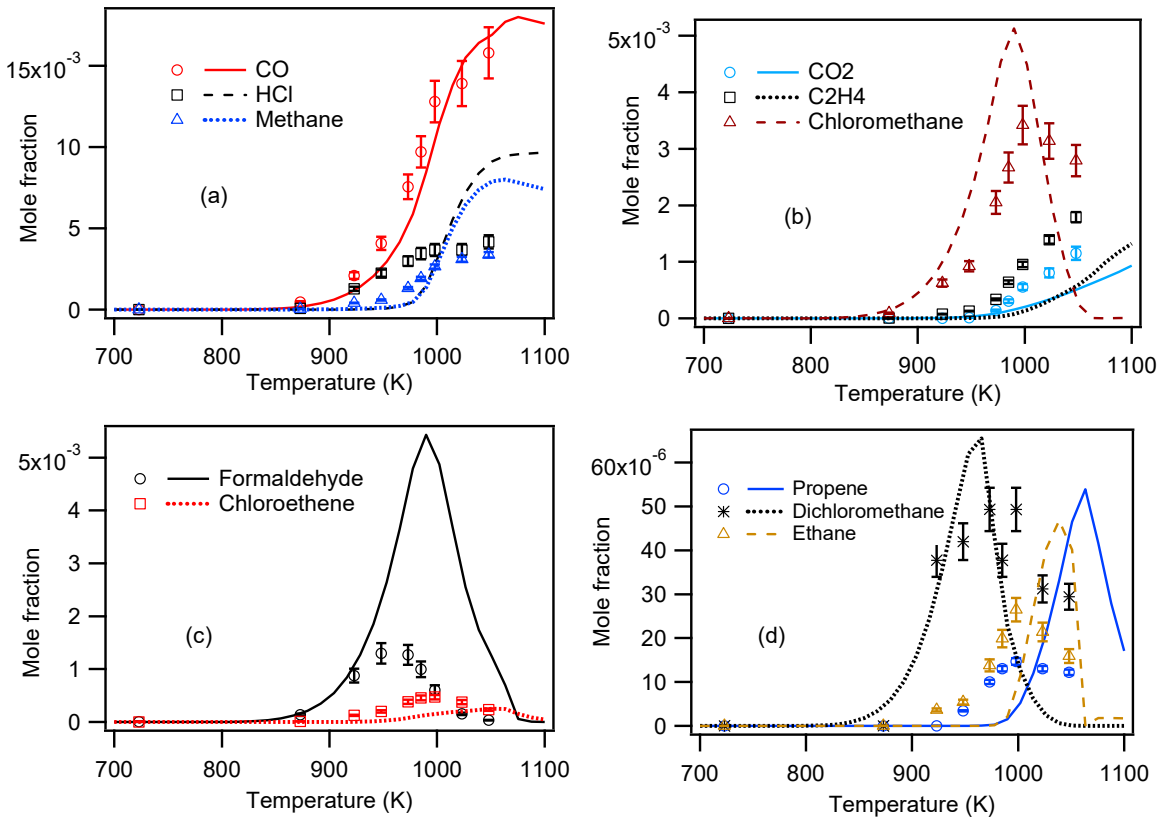

Figure 5. Mole fraction evolution with temperature in the TR of (a) CO/HCl/methane, (b) CO_2/C_2H_4/chloromethane, (c) formaldehyde/chloroethene, and (d) propene/dichloromethane/ethane (MC inlet mole fraction of 0.01, residence time of 2 s, and P = 1.07 bar).

5. Discussion

Because the model reproduces in an acceptable way the TR experimental results, a flow rate analysis has been performed at 1000 K using the OpenSMOKE package (Figure 6).

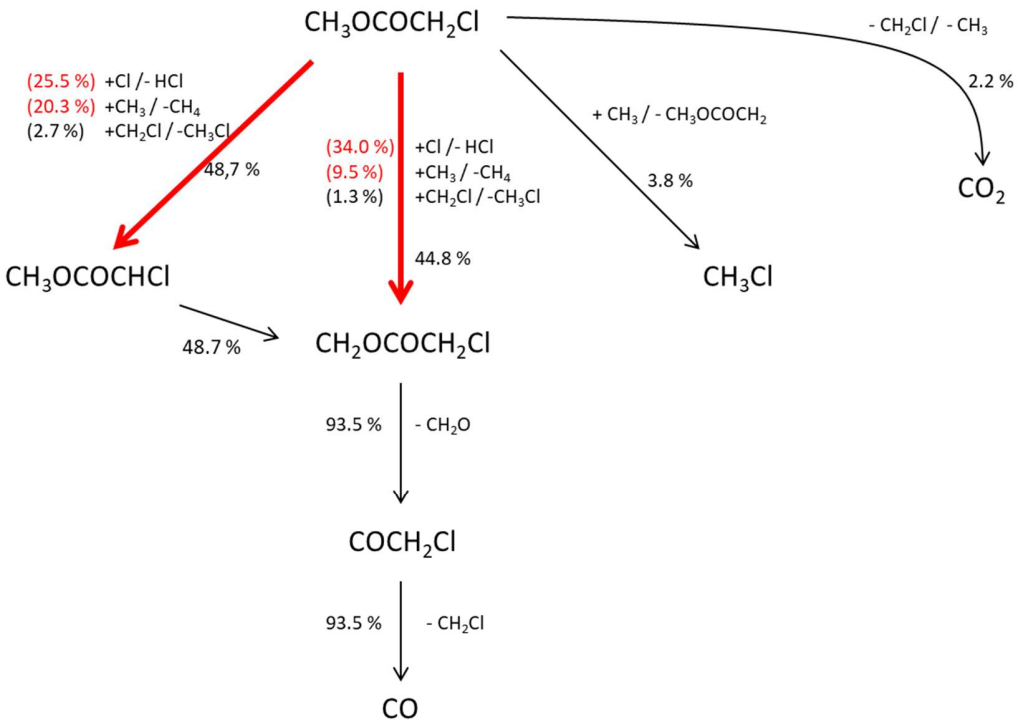

Figure 6. Simplified flow rate analysis at 1000 K (MC inlet mole fraction of 0.01, residence time of 2 s, and P = 1.07 bar). Numbers on arrows represent the consumption rates normalized by the total MC consumption rate. Red thick arrows correspond to the main ways of decomposition of MC. Consumption rates lower than 1% are not represented.

According to the flow rate analysis, the major consumption pathways of MC decomposition are:

- H-atom abstraction by CH_3, Cl, and CH_2Cl atoms leading to the formation of $CH_3OCOCHCl$, chloromethane, methane, and HCl (48.7%, reactions 14, 19, and 25 in Table 1, respectively),
- H-atom abstraction by the same radicals leading to the formation of CH_2OCOCH_2Cl, chloromethane, methane, and HCl (44.8%, reactions 16, 21, and 27 in Table 1, respectively)

The most important H-atom abstractions at 1000 K are those by Cl atoms (59.5%) which include these two H-atom abstractions:

- $CH_3OCOCH_2Cl + Cl = CH_3OCOCHCl + HCl$ (25.5%, reaction 19 in Table 1),
- $CH_3OCOCH_2Cl + Cl = CH_2OCOCH_2Cl + HCl$ (34.0%, reaction 21 in Table 1).

Next, H-atom abstractions by methyl radicals contribute to 29.8% of the MC consumption rate:

- $CH_3OCOCH_2Cl + CH_3 = CH_3OCOCHCl + CH_4$ (20.3%, reaction 14 in Table 1),

- $CH_3OCOCH_2Cl + CH_3 = CH_2OCOCH_2Cl + CH_4$ (9.5%, reaction 16 in Table 1).

Finally, H-atom abstractions by CH2Cl radicals account for 4.0% of the MC consumption rate:

- $CH_3OCOCH_2Cl + CH_2Cl = CH_3OCOCHCl + CH_3Cl$ (2.7%, reaction 25 in Table 1),
- $CH_3OCOCH_2Cl + CH_2Cl = CH_2OCOCH_2Cl + CH_3Cl$ (1.3%, reaction 27 in Table 1).

The $CH_3OCOCHCl$ radical decomposes totally by isomerization, forming CH_2OCOCH_2Cl (reaction 35 in Table 1) as shown in Figure 6. The latter can react by β-scission to give formaldehyde and $COCH_2Cl$ radical (reaction 31 in Table 1), which decomposes by α-scission reaction yielding to the formation of CO and CH_2Cl radical (reaction 33 in Table 1).

The minor pathways of MC thermal decomposition include the following:

- Cl-atom abstraction by CH_2Cl radical leading to the formation of dichloromethane and CH_3OCOCH_2 radical (reaction 18 in Table 1),
- decomposition reaction of MC giving CO_2 and CH_2Cl and CH_3 radicals (reaction 5 in Table 1).

Concerning minor products, propene formation comes from the reaction between methyl radical and ethylene. Cl-atom abstractions with CH_2Cl from the reactive lead to the formation of dichloromethane. The production of ethane is mainly due to the H-atom abstraction by ethyl radical from chloromethane. Elimination of HCl from dichloroethane explains the formation of vinyl chloride. Formation of dichloroethane results from the termination between two CH_2Cl radicals. Note that, under the conditions of this study, CO_2 does not arise from the oxidation of CO but from the fuel unimolecular initiation. The underestimation of formaldehyde mole fractions by the model could be due to the use of inaccurate kinetic parameters for the consumption of this species, but not to a wrong relative ratio between the two radicals formed from the fuel since $CH_3OCOCHCl$ totally isomerizes yielding the second one, CH_2OCOCH_2Cl, which leads to formaldehyde and carbon monoxide.

To better understand the most influential reactions, a sensitivity analysis at 1000 K is shown in Figure 7.

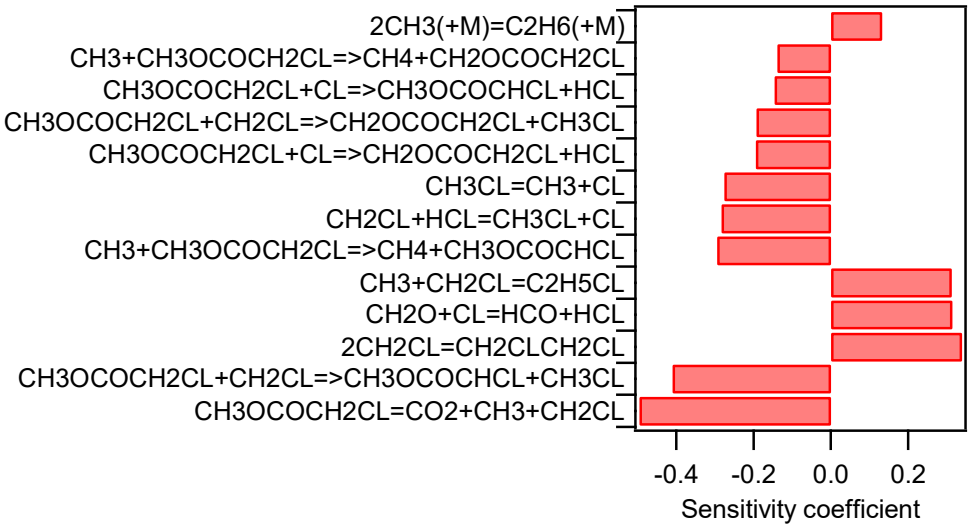

Figure 7. Sensitivity analysis on MC mole fraction at 1000 K (MC inlet mole fraction of 0.01, residence time of 2 s, and P = 1.07 bar). Reactions with a negative coefficient have a promoting effect on the reactivity.

The reactions with the largest promoting effect at 1000 K are as follows:

- decomposition of MC into CO_2 and CH_3 and CH_2Cl radicals (reaction 5 in Table 1) by producing two important radicals in the system,
- H-atom abstraction with CH_2Cl from MC (reactions 25 and 27 in Table 1).

H-atom abstractions with methyl radicals and Cl-atoms from MC have also an important promoting effect on the reactivity (reactions 14, 16, 19, and 21 in Table 1). Furthermore, the decomposition of chloromethane $CH_3Cl = CH_3 + Cl$ also enhances the reactivity by producing two important radicals in the system. Since the most important H-atom abstraction involves Cl radicals at 1000 K, the following reaction, $CH_2Cl + HCl = CH_3Cl + Cl$, promotes the reactivity by producing Cl atoms.

Termination reactions between two CH_2Cl radicals and between methyl and CH_2Cl radicals, leading respectively to dichloroethane and chloroethane, have an inhibiting effect on the reactivity since those reactions are radical consuming. The H-atom abstraction from formaldehyde with Cl atoms producing HCO and HCl has also an inhibiting effect on the MC decomposition by consuming Cl atoms.

6. Extrapolation of the Results to the Case of Ethyl Bromoacetate

To give an idea about the extrapolation of the results obtained with the methyl chloroacetate to the chemical warfare agent (Figure 1), simulations were run with a version of the model developed in this study just modified taking into account the bond dissociation energy difference between C–Cl and C–Br. The differences induced by the presence of an ethyl group instead of a methyl one were considered as being of second order, even if, for a halogenated ethyl ester, the molecular decomposition yielding ethylene and halogenated acetic acid should be taken into account for a more accurate modeling. Therefore, the main difference between the two molecules is the nature of the halogen atom: bromide and chloride (written X in the following sentences). The C–X bond dissociation energy is different depending on the halogen involved (70.3 kcal/mol for the C–Br bond in bromoethane and 83.7 for the C–Cl bond in chloromethane for example) [27]. This bond energy difference (about 13 kcal/mol) affects directly the activation energy of several reaction types, mainly the unimolecular initiation reaction by breaking of the C–X bond. Consequently, on line with the Evans–Polanyi approach [28], the activation energy of the unimolecular initiation by breaking of the C–Cl bond has been lowered by 13 kcal/mol to provide a reasonable prediction of the reactivity of the ethyl bromoacetate. This approach based on bond energy has been proven successful when modeling diethyl ether and diethyl sulfide [29]. The results obtained with this modification are shown in Figure 8.

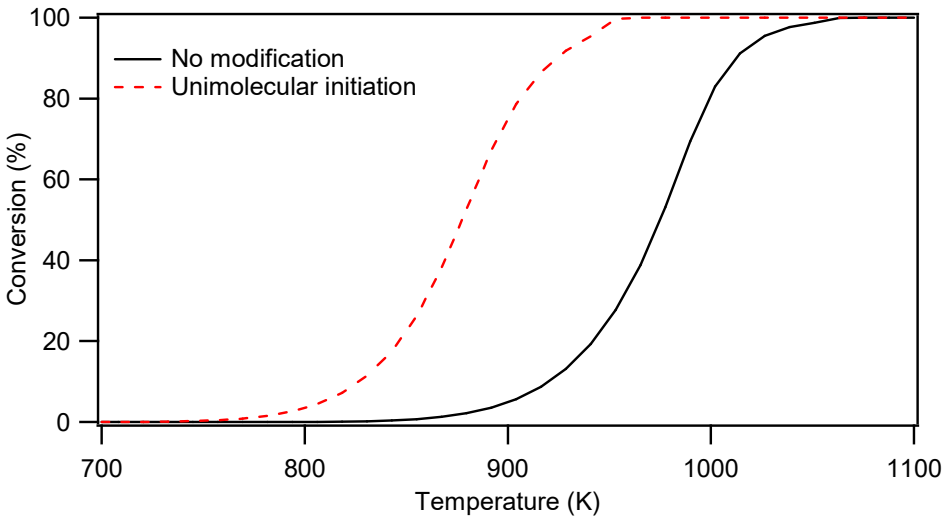

Figure 8. Evolution with temperature of MC conversion (MC inlet mole fraction of 0.01, residence time of 2 s, and P = 1.07 bar). The black line is a simulation performed with the initial kinetic model; the red line is a simulation performed with the activation energy of the reaction CH_3OCOCH_2Cl = CH_3OCOCH_2 + Cl lowered by 13 kcal/mol.

We can observe that the reactivity of the system is very sensitive to the value of the activation energy of unimolecular initiation by breaking of the C–X bond. The lowering by 13 kcal/mol leads to a significant shift of the reactivity (about 100 K) toward lower temperatures, meaning that ethyl bromoacetate is more reactive than methyl chloroacetate. The onset and full conversion temperatures of the thermal decomposition of ethyl bromoacetate should occur at lower temperatures (100 K lower) than those for the methyl chloroacetate. Of course, this is only a first rough attempt of modeling the pyrolysis of ethyl bromoacetate and a more accurate investigation will require the development of a model specific for this molecule, but this is beyond the scope of this work.

7. Conclusion

This work presents the first pyrolysis study of a halogenated ester, methyl chloroacetate (MC). It was performed in a tubular reactor at temperatures ranging from 573 to 1048 K and at a fixed residence time of 2 s. The inlet MC mole fraction was fixed at 0.01. All experiments were conducted at 1.07 bar. Thanks to the use of gas chromatography and FTIR spectroscopy, the following products were quantified: CO, HCl, methane, CO_2, C_2H_4, chloromethane, formaldehyde, vinyl chloride, propene, dichloromethane, and ethane. Traces of dichloroethane, ethyl acetate, methanol, acetaldehyde, 1,3-butadiene, 1-chloropropene, methyl formate, and water were also found.

In this study, a detailed kinetic model was developed and tested against our experimental results. Mole fractions of CO, chloromethane, CO_2, and dichloromethane are well-reproduced by the kinetic model. Some discrepancies between experimental and modeling results are encountered for minor products. The large numbers of kinetic parameters estimated in the kinetic model could partly explain these deviations. The kinetic analysis of the model shows that the major consumption pathways during the pyrolysis of MC are (1) the H-atom abstractions by the CH_2Cl radical and (2) the unimolecular initiation reaction of MC yielding CO_2, CH_3 and CH_2Cl.

A first approach of the extrapolations to the actual chemical warfare agent reveals that the brominated compound should be destroyed at a temperature about 100 K lower than the chlorinated one, which is fully consumed at 1048 K under our experimental conditions.

Supplementary Material

Kinetic mechanism used in this work given under CHEMKIN format.

Thermodynamic data of all species of the mechanism.

Scheme of the experimental setup used for running pyrolysis experiments, measured temperature profile in the TR in absence of reaction, and the carbon, oxygen, and chlorine balances, SCF energy, zero-point corrected electronic energy, frequencies and geometry of molecules, radicals and transition states, calculated at the CBS-QB3 level of theory, comparison of the kinetic parameters of reaction R30 in Table 1 with literature data, experimental mole fractions of species in a tabular form.

References

(1) Wang, X.-F.; Hai, X.; Shu, Y.; Chen, X.-W.; Wang, J.-H. A Novel Cross-Linked Co-Polymeric Ionic Liquid as a Potential Adsorbent for Highly Efficient Adsorption of Curcuminoids. Anal. Methods 2015, 7 (22), 9529–9534. https://doi.org/10.1039/C5AY02308D.

(2) Hu, K.; Zhao, D.; Wu, G.; Ma, J. Polyesters Derived from Bio-Based Eugenol and 10-Undecenoic Acid: Synthesis, Characterization, and Structure–Property Relationships. RSC Adv. 2015, 5 (105), 85996–86005. https://doi.org/10.1039/C5RA17457K.

(3) Lloyd, A. W.; Olliff, C. J.; Rutt, K. J. A Study of Modified Betaines as Cryoprotective Additives. J. Pharm. Pharmacol. 1994, 46 (9), 704–707. https://doi.org/10.1111/j.2042-7158.1994.tb03887.x.

(4) Tedesco, D.; Fabini, E.; Barbakadze, V.; Merlani, M.; Zanasi, R.; Chankvetadze, B.; Bertucci, C. Stopped-Flow Enantioselective HPLC-CD Analysis and TD-DFT Stereochemical Characterization of Methyl Trans-3-(3,4-Dimethoxyphenyl)Glycidate. Chirality 2015, 27 (12), 914–918. https://doi.org/10.1002/chir.22539.

(5) Wang, T.; Tang, J.; Wan, W.; Zhao, S. Methyl Chloroacetate as an Extraction Solvent for Coupling Liquid–Liquid Semimicroextraction with Micellar Electrokinetic Chromatography through on-Capillary Decomposition for the Separation of Neutral Compounds with Concentration Enhancement. J. Chromatogr. A 2007, 1147 (1), 105–110. https://doi.org/10.1016/j.chroma.2007.02.025.

(6) Schneider, J. F. Chemical Weapons Destruction and Explosive Waste/Unexploded Ordnance Remediation. Robert Noyes, Noyes Publications, 369 Fairview Avenue, Westwood, NJ 07675, (1996), 235 Pages, [ISBN: 0-8155-9], U.S. List Price: $64.00. Environ. Prog. 1999, 18 (1), S7–S8. https://doi.org/10.1002/ep.670180106.

(7) Preuss, J. The Reconstruction of Production and Storage Sites for Chemical Warfare Agents and Weapons from Both World Wars in the Context of Assessing Former Munitions Sites. In One Hundred Years of Chemical Warfare: Research, Deployment, Consequences; Friedrich, B., Hoffmann, D., Renn, J., Schmaltz, F., Wolf, M., Eds.; Springer International Publishing, 2017; pp 289–333.

(8) Battin-Leclerc, F.; Baronnet, F.; Paternotte, G.; Leclerc, J. P.; Gourhan, R. Thermal Decomposition of Chloropicrin, Diphosgene and Phosgene between 100 and 530°C. J. Anal. Appl. Pyrolysis 2000, 53 (1), 95–105. https://doi.org/10.1016/S0165-2370(99)00052-2.

(9) Conesa, J. A.; Font, R.; Fullana, A.; Martín-Gullón, I.; Aracil, I.; Gálvez, A.; Moltó, J.; Gómez-Rico, M. F. Comparison between Emissions from the Pyrolysis and Combustion of Different Wastes. J. Anal. Appl. Pyrolysis 2009, 84 (1), 95–102. https://doi.org/10.1016/j.jaap.2008.11.022.

(10) Farooq, A.; Davidson, D. F.; Hanson, R. K.; Huynh, L. K.; Violi, A. An Experimental and Computational Study of Methyl Ester Decomposition Pathways Using Shock Tubes. Proc. Combust. Inst. 2009, 32 (1), 247–253. https://doi.org/10.1016/j.proci.2008.06.084.

(11) Peukert, S. L.; Sivaramakrishnan, R.; Su, M.-C.; Michael, J. V. Experiment and Theory on Methylformate and Methylacetate Kinetics at High Temperatures: Rate Constants for H-Atom Abstraction and Thermal Decomposition. Combust. Flame 2012, 159 (7), 2312–2323. https://doi.org/10.1016/j.combustflame.2012.03.007.

(12) Yang, X.; Felsmann, D.; Kurimoto, N.; Krüger, J.; Wada, T.; Tan, T.; Carter, E. A.; Kohse-Höinghaus, K.; Ju, Y. Kinetic Studies of Methyl Acetate Pyrolysis and Oxidation in a Flow Reactor and a Low-Pressure Flat Flame Using Molecular-Beam Mass Spectrometry. Proc. Combust. Inst. 2015, 35 (1), 491–498. https://doi.org/10.1016/j.proci.2014.05.058.

(13) Ren, W.; Lam, K.-Y.; Davidson, D. F.; Hanson, R. K.; Yang, X. Pyrolysis and Oxidation of Methyl Acetate in a Shock Tube: A Multi-Species Time-History Study. Proc. Combust. Inst. 2017, 36 (1), 255–264. https://doi.org/10.1016/j.proci.2016.05.002.

(14) Vin, N.; Battin-Leclerc, F.; Le Gall, H.; Sebbar, N.; Bockhorn, H.; Trimis, D.; Herbinet, O. A Study of Chlorobenzene Pyrolysis. Proc. Combust. Inst. 2018. https://doi.org/10.1016/j.proci.2018.05.067.

(15) Vin, N.; Battin-Leclerc, F.; Herbinet, O. A Study of Thermal Decomposition of Bromoethane. J. Anal. Appl. Pyrolysis 2018. https://doi.org/10.1016/j.jaap.2018.10.005.

(16) Cuoci, A.; Frassoldati, A.; Faravelli, T.; Ranzi, E. OpenSMOKE++: An Object-Oriented Framework for the Numerical Modeling of Reactive Systems with Detailed Kinetic Mechanisms. Comput. Phys. Commun. 2015, 192, 237–264. https://doi.org/10.1016/j.cpc.2015.02.014.

(17) Zhou, C.-W.; Li, Y.; O'Connor, E.; Somers, K. P.; Thion, S.; Keesee, C.; Mathieu, O.; Petersen, E. L.; DeVerter, T. A.; Oehlschlaeger, M. A.; et al. A Comprehensive Experimental and Modeling Study of Isobutene Oxidation. Combust. Flame 2016, 167, 353–379. https://doi.org/10.1016/j.combustflame.2016.01.021.

(18) Pelucchi, M.; Frassoldati, A.; Faravelli, T.; Ruscic, B.; Glarborg, P. High-Temperature Chemistry of HCl and Cl2. Combust. Flame 2015, 162 (6), 2693–2704. https://doi.org/10.1016/j.combustflame.2015.04.002.

(19) Frisch, M. J. Gaussian 09,.

(20) Montgomery, J. A.; Frisch, M. J.; Ochterski, J. W.; Petersson, G. A. A Complete Basis Set Model Chemistry. VI. Use of Density Functional Geometries and Frequencies. J. Chem. Phys. 1999, 110 (6), 2822–2827. https://doi.org/10.1063/1.477924.

(21) Becke, A. D. Density-functional Thermochemistry. III. The Role of Exact Exchange. J. Chem. Phys. 1993, 98 (7), 5648–5652. https://doi.org/10.1063/1.464913.

(22) Private Communication.

(23) Mereau, R.; Rayez, M. T.; Rayez, J. C.; Caralp, F.; Lesclaux, R. Theoretical Study on the Atmospheric Fate of Carbonyl Radicals: Kinetics of Decomposition Reactions. Phys. Chem. Chem. Phys. 2001, 3 (21), 4712–4717. https://doi.org/10.1039/b105824j.

(24) Shilov, A. E.; Sabirova, R. D. Mechanism of the Primary Act of the Thermal Decomposition of Methane Derivatives. 1959, 6.

(25) Burcat, A. Third Millennium Ideal Gas and Condensed Phase Thermochemical Database for Combustion with Updates from Active Thermochemical Tables.

(26) Muller, C.; Michel, V.; Scacchi, G.; Côme, G. M. THERGAS: A Computer Program for the Evaluation of Thermochemical Data of Molecules and Free Radicals in the Gas Phase. J. Chim. Phys. 1995, 92, 1154–1178. https://doi.org/10.1051/jcp/1995921154.
(27) Luo, Y.-R. Comprehensive Handbook of Chemical Bond Energies; CRC Press, 2007.
(28) Evans, M. G.; Polanyi, M. Inertia and Driving Force of Chemical Reactions. Trans. Faraday Soc. 1938, 34 (0), 11–24. https://doi.org/10.1039/TF9383400011.
(29) Vin, N.; Herbinet, O.; Battin-Leclerc, F. Diethyl Ether Pyrolysis Study in a Jet-Stirred Reactor. J. Anal. Appl. Pyrolysis 2016, 121, 173–176. https://doi.org/10.1016/j.jaap.2016.07.018.
(30) Bounaceur, R.; Warth, V.; Marquaire, P.-M.; Scacchi, G.; Dominé, F.; Dessort, D.; Pradier, B.; Brevart, O. Modeling of Hydrocarbons Pyrolysis at Low Temperature. Automatic Generation of Free Radicals Mechanisms. J. Anal. Appl. Pyrolysis 2002, 64 (1), 103–122. https://doi.org/10.1016/S0165-2370(01)00173-5.
(31) Huynh, L. K.; Violi, A. Thermal Decomposition of Methyl Butanoate: Ab Initio Study of a Biodiesel Fuel Surrogate. J. Org. Chem. 2008, 73 (1), 94–101. https://doi.org/10.1021/jo701824n.
(32) Zhou, Y. Z.; Li, S.; Li, Q. S.; Zhang, S. W. Theoretical Investigation of the Decarboxylation Reaction of CH3CO2 Radical. J. Mol. Struct. THEOCHEM 2008, 854 (1), 40–45. https://doi.org/10.1016/j.theochem.2007.12.033.
(33) Maricq, M. M.; Ball, J. C.; Straccia, A. M.; Szente, J. J. A Diode Laser Study of the Cl + CH3CO Reaction. Int. J. Chem. Kinet 1997, 29 (6), 421–429. https://doi.org/10.1002/(SICI)1097-4601(1997)29:6<421::AID-KIN3>3.0.CO;2-W.
(34) Senosiain, J. P.; Klippenstein, S. J.; Miller, J. A. Pathways and Rate Coefficients for the Decomposition of Vinoxy and Acetyl Radicals. J. Phys. Chem. A 2006, 110 (17), 5772–5781. https://doi.org/10.1021/jp054934r.